LA-U... 92-1360

Title: FOIL OPTIMIZATION FOR LOW ENERGY NEUTRAL ATOM IMAGING

LA-UR--92-1360

DE92 013435

Author(s): Herbert O. Funsten, David J. McComas, and Bruce L. Barraclough

Submitted to: SPI's Symposium: Instrumentation for Magnetospheric Imagery, 19-24 July 1992, San Diego, CA

This report was prepared as an account of work sponsored by an agency of the United States Government. Neither the United States Government nor any agency thereof, nor any of their employees, makes any warranty, express or implied, or assumes any legal liability or responsibility for the accuracy, completeness, or usefulness of any information, apparatus, product, or process disclosed, or represents that its use would not infringe privately owned rights. Reference herein to any specific commercial product, process, or service by trade name, trademark, manufacturer, or otherwise does not necessarily constitute or imply its endorsement, recommendation, or favoring by the United States Government or any agency thereof. The views and opinions of authors expressed herein do not necessarily state or reflect those of the United States Government or any agency thereof.

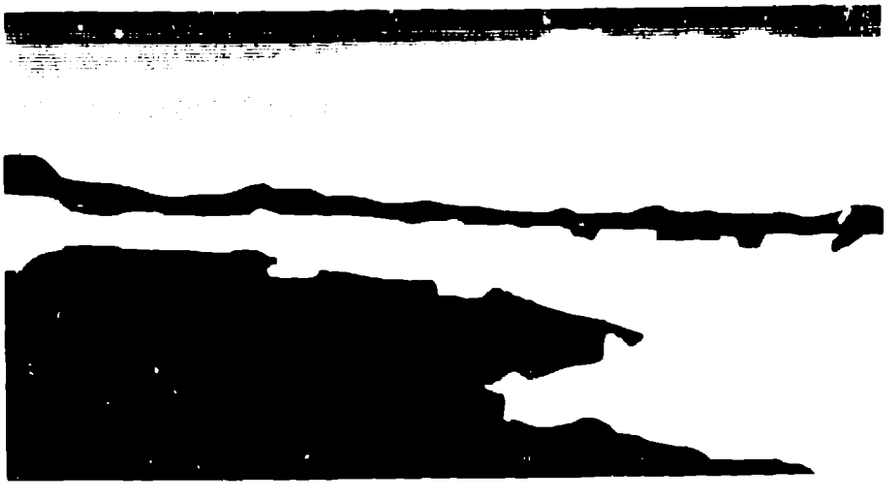

Los Alamos
NATIONAL LABORATORY

Los Alamos National Laboratory, an affirmative action/equal opportunity employer, is operated by the University of California for the U.S. Department of Energy under contract W-7405-ENG-36. By acceptance of this article, the publisher recognizes that the U.S. Government retains a nonexclusive, royalty-free license to publish or reproduce the published form of this contribution, or to allow others to do so, for U.S. Government purposes. The Los Alamos National Laboratory requests that the publisher identify this article as work performed under the auspices of the U.S. Department of Energy.

MASTER

Foil Optimization for Low Energy Neutral Atom Imaging

Herbert O. Funsten, David J. McComas, and Bruce L. Barraclough

Space Plasma Physics Group, MS D438

Los Alamos National Laboratory

Los Alamos, NM 87545

ABSTRACT

Magnetospheric imaging has been proposed using remote detection of low energy neutral atoms (LENAs) of magnetospheric origin. In the detector, LENAs can be removed from the immense ambient EUV by charge modification (ionization) using a carbon stripping foil and can be subsequently deflected into an E/q analysis section. The detector sensitivity efficiency of LENAs is highly dependent on the ionization probability of neutrals as they transit the carbon foil. In this study, we present equilibrium charge state distributions and scatter distributions for 1-30 keV atomic hydrogen and oxygen transiting 0.5 $\mu g\ cm^{-2}$ carbon foils. The fraction of hydrogen exiting a foil as H^+ ranges from approximately 5% at 1 keV to 41% at 30 keV. The fraction of oxygen exiting the foil as O^+ ranges from 2% at 10 keV to 8% at 30 keV. Results obtained after coating the exit surface of foils with either aluminum (which forms aluminum oxide when exposed to air) or gold suggests that the exit surface chemistry has no effect on the charge state distributions due to foil contamination from exposure to air. Scattering resulting from the atom-foil interaction is shown to be independent of the charge state distribution, suggesting that the interaction mechanisms resulting in charge exchange and scattering are distinctly different.

1. INTRODUCTION

The terrestrial magnetosphere has been extensively studied using *in situ* data acquired along various spacecraft orbits. Unfortunately, interpretation of such single-point measurements is ambiguous due to dynamic variations of the magnetosphere. Remote imaging of the magnetosphere has been proposed by detection of energetic neutral atoms (ENAs) and low energy neutral atoms (LENAs) which are created by neutralization of magnetospheric ions (predominantly hydrogen and some oxygen) with geocoronal neutral species. Since ENAs and LENAs do not interact with local electromagnetic fields, they obtain a straight trajectory and can be detected remotely. A remote, orbiting LENA detector should provide trajectory and energies information to map the plasma source locations, strengths, and energy distributions (see Moore, *et al.*, these proceedings).

Detection of ENAs and LENAs of magnetospheric origin requires their removal from immense fluxes of ambient EUV ($\approx 10^{10}$ $cm^{-2}s^{-1}$). ENAs can either be directly detected by a solid state detector which is insensitive to EUV [RWM] or removed from the EUV by transiting thick carbon blocking foil which is opaque to EUV [RWM,KCH]. However, due to their low energies LENAs cannot be detected by solid state detectors and will not transit a thick blocking foil without severe energy straggling and angular scattering. Removal of LENAs from the ambient EUV can performed by first ionizing them and subsequently electrostatically deflecting them from the ambient EUV into an energy-angle measurement section of the imager (see McComas *et al.*, these proceedings). Obviously, the sensitivity of the imager depends highly on the ionization efficiency of the charge stripper.

A straightforward method of LENA charge modification utilizes ultrathin carbon foils for charge stripping [DJM91]. Carbon foils are structurally robust and can withstand the severe conditions of launch and harsh environment of space. Ultra-thin foils of nominal thickness 0.5 $\mu g\ cm^{-2}$ can be employed to minimize angular scattering and energy straggling of LENAs in the foils. In this study we present experimental results describing the equilibrium charge state and scatter distributions of low energy (1 to 30 keV) atomic hydrogen and oxygen which transit ultrathin (0.5 $\mu g\ cm^{-2}$) foils. We demonstrate that coating of the surface with either gold or aluminum has no observable effect on the hydrogen charge state distributions. The results of the charge state distributions, which are

independent of foil thickness, are directly applicable to techniques using blocking foils.

2. EXPERIMENTAL APPARATUS

The experimental apparatus used in this study, which is illustrated in Fig. 1 and is similar to the apparatus used by Burgi et al. [BURG], allows for both charge state and angular scattering analysis of the transiting beam. Ions were generated in a duoplasmatron ion source, accelerated to an energy of 1 keV to 30 keV, and magnetically analyzed. The ions passed through a 1 mm diameter beam-defining aperture located 12.5 mm upstream of a foil holder which held 5 foils, each of which could be moved into the beam by a micropositioner. After transiting the foil, the initially collimated ion beam is composed of scattered ions and neutrals. Some of these atoms pass through a 0.35 x 25 mm horizontal (see Fig. 1) slit located 30 mm behind the foil. Since the center of the slit corresponds to the beam axis, the horizontal distribution of atoms contains direct information about the angular scattering of the atoms in the foil. Ions which pass through the slit are vertically E/q analyzed by a pair of deflection plates. All atoms which pass through the slit subsequently strike an imaging microchannel plate (IMCP) detector located 70 mm behind the slit. Neutrals, which are not deflected, strike a central region of the IMCP detector, whereas ionized species are deflected toward outer regions of the IMCP detector. The vertical position of the negative, neutral, and positive charge state distributions is a function of the deflection voltage and the charge state of the ions. A background subtraction was performed on the integrated charge state distributions, which were then converted into a fraction relative to the other charge states.

Ultra-thin foils used in this study can have pinholes which will detrimentally affect analysis of the scatter and charge state distributions. However, incident ions (with charge state +1) which transit a hole are neither scattered nor charge modified and will therefore be observed as a localized high-count region in the center of the +1 charge state distribution. Using the IMCP detector, the high-count region corresponding to a hole can be detected, and during subsequent analysis this region can easily be avoided. In fact, using a new technique of Transmitted Ion Mapping, such structural flaws can be observed and optimal foils can be selected [FUN].

The final charge state of atoms exiting a surface has been shown to be sensitive to the exit surface chemistry [KREU,BEHR,BERK]. To observe if coatings affected the exit charge state of transiting atoms, Al and Au layers were deposited on the exit surface of the carbon foils. These layers, each 17 Å thick, were deposited by evaporation in a vacuum chamber at 6×10^{-6} torr. Upon exposure to air, the Al layer immediately forms aluminum oxide. These foils were installed into the vacuum chamber one day after Al or Au deposition and allowed to pump for several days at a pressure of 5×10^{-8} torr.

3. EXIT CHARGE STATE DISTRIBUTION

As an atomic beam traverses a foil, the charge state composition changes due to electron loss and capture events associated with the interaction of the transiting particle and the atoms in the foil. After a certain number of interactions, which corresponds to a penetration depth λ, an equilibrium charge state distribution will be established. Extrapolating empirical charge equilibration depths at derived at somewhat higher energies [BETZ], charge equilibration of incident ions at the energies used in this study should occur within a distance $\lambda < 4$ Å (≈ 0.1 μg/cm^2) into the carbon foil. At this point, the beam retains no information of its initial charge state. Since λ is less than the thickness of the foils used in this study (i.e., charge equilibration has occurred), we can extend our results using an incident ions (H^+ and O^+) to incident neutrals.

Equilibrium charge state distributions of incident H^+ or O^+ that transited 0.5 μg/cm^2 carbon foils are depicted in Figs. 2 and 3, respectively. The solid lines in the figures represent a quadratic least squares fit to the data. The results of the empirical fit are:

$$f(H^+) = -3.24x10^{-4}E^2 + 0.222E + 0.0342 \quad (1a)$$

$$f(O^+) = 2.86x10^{-3}E - 5.79x10^{-3} \quad (1b)$$

$$f(O^-) = -2.58x10^{-4}E^2 + 0.0124E + 0.0418 \quad (1c)$$

The charge states are plotted as a function of incident ion energy, since energy straggling is expected to be small **NOTE: EXPOUND.**

For hydrogen, the fraction of the beam exiting the foil as protons $f(H^+)$ increases with increasing energy, whereas the charge state fraction $f(H^-)$ reaches a maximum at approximately $E_0 = 4$ keV and subsequently decreases with increasing energy. Based on counting statistics, the error is less than 0.5%. However, at high energies a reproducible discrepancy of 4% was observed, so Fig. 2 shows the average of the two results. The values of $f(H^+)$ presented here agree with the results of Kreussler and Sizmann [ ] who derived an empirical relationship for incident proton energies 50-230 keV

$$f(H^-) \approx 1 - f(H^0) \quad (2a)$$

$$\approx 1 - \exp(-1.07x^2 + 0.69x + 4.08) \quad (2b)$$

where $x = \ln(1+0.7v/v_0)$ and v is the exit velocity of the transiting projectile and v_0 is the Bohr velocity.

For oxygen, both the fraction of O^+ and O^- increase with increasing energy, although the rate of increase for $f(O^-)$ decreases (at energies higher than those used in this study, $f(O^-)$ is expected to rapidly decrease). The fraction $f(O^-)$ shows a large, random variation which was similarly observed in Burgi *et al.* [ ], although their results for $f(O^+)$ and $f(O^-)$ were 40% higher than this study. Since the fractions of O^- and H^+ are the largest charge state in this energy regime, an ideal LENA detector should be designed for neutral conversion to, and subsequent detection of, O^- and H^+.

The effect of the exit surface chemistry, and therefore the possibility of enhancing the ionization yield, was investigated by vapor depositing Al or Au layers on the exit surfaces of foils. Fig. 4 shows a comparison of the exit charge state distributions $f(H^+)$ of incident H^+ on coated foils relative to

uncoated foils. If we define f_C as the fraction $f(H^+)$ from uncoated (carbon) foils and f_X as the fraction $f(H^+)$ emitted from foils coated with either aluminum (f_{Al}) or gold (f_{Au}), then the variation between coated and uncoated foils is $(f_C-f_X)/f_C$. As shown in Fig. 4, the variation of the charge state distributions is less than approximately 2% and is not systematic. Therefore, the charge state distributions of coated and uncoated foils are virtually identical, demonstrating that the exit charge state distribution for incident hydrogen is *independent* of the exit surface chemistry. This is apparently the result of foil history. The coated foils were exposed to atmosphere for approximately one day between their Al or Au deposition and installation into the experimental chamber. This apparently results in surface contamination of the deposited layers. Since all foils were "dirty", they exhibited identical charge state distributions. This has been previously observed in "dirty" foils [KREU.BEHR.BERK], and only "clean" foils with layers deposited *in situ* showed a variation in their charge state distributions. However, *in situ* deposition of exit surface layers has been shown to increase the charge state fraction by approximately 5-10%, so the surface chemistry is a relatively minor chemical effect. Since foils would be exposed to air at some point during the LENA sensor assembly and calibration process, we expect all foils to generate charge state distributions identical to those depicted in Fig. 4.

4. ANGULAR SCATTERING

Angular scattering of atoms that transit foils can result in degraded instrument sensitivity since information about their incident trajectories is lost. For example, large angular scattering in the carbon stripping foil in the apparatus described in McComas *et al.* (these proceedings) would result in a significantly reduced throughput of the energy analyzer/deflection section. Consequently, investigation of projectile-foil scattering is vital in the design of the LENA detector.

A semi-empirical theory describing multiple, low angle scattering was derived by Meyer [MEYER] and has in general been experimentally verified [HOGLANDE.BERN]. We consider a projectile of

atomic mass m_1 and atomic number Z_1 incident at an initial energy E on a foil with atomic mass m_2, atomic number Z_2, thickness t, and atomic density N. The Meyer theory defines the reduced thickness (τ), the reduced scattering angle (ψ), and the reduced energy (ϵ) as

$$\tau = \pi a^2 N t \tag{3a}$$

$$\psi = \psi \frac{\epsilon}{2} \frac{m_1 + m_2}{m_2} \tag{3b}$$

$$\epsilon = \frac{aEm_2}{Z_1 Z_2 e^2 (m_1 + m_2)} \tag{3c}$$

where e is the unit charge, ψ is the scattering angle in the laboratory frame, and a, which is the Thomas-Fermi screening parameter, equals 0.885 $a_0(Z_1^{2/3} + Z_2^{2/3})^{-1/2}$ where a_0 is the Bohr radius (0.529 Å).

Based on the Meyer theory, a unique, energy-independent reduced half-angle $\psi_{1/2}$ exists for every reduced foil thickness τ, which is dependent only on Z_1, Z_2, N, and t. Consequently, if we can determine $\psi_{1/2}$ using the Meyer theory for a given projectile-foil combination, we can predict the scattering half-angle according to the equation:

$$\psi_{\frac{1}{2}} = \psi_{\frac{1}{2}} \frac{2Z_1 Z_2 e^2}{aE} \tag{4}$$

This equation illustrates that $\psi_{1/2}$ is inversely proportional to the projectile energy for any given projectile-foil system. For a 0.5 $\mu g/cm^2$ carbon foil, the reduced thickness for incident H and O are 0.4014 and 0.2365, respectively, which corresponds to $\psi_{1/2}$ = 0.121 for H and 0.0654 for incident O.

Figure 5 depicts the scattering half-angle $\psi_{1/2}$ derived in this study (points) and calculated using the Meyer theory (solid line). The empirical data of this study is approximately a factor of 2-3 greater for H and 4-5 for O than predicted by the Meyer theory. A fit of the hydrogen data to the Meyer theory, which results in $\psi_{1/2}$ = 12.6/E(keV) (dashed line), implies a film thickness of 1.16 $\mu g\ cm^{-2}$. This may be the result of a greater foil thickness than cited by the manufacturer. In fact, the thickness error cited by the manufacturer for 0.5 $\mu g\ cm^{-2}$ foils is $\pm 0.5\ \mu g\ cm^{-2}$.

Fig. 6 depicts the scatter distributions at the IMCP detector for charge states of H^0 and H^+ at 20 keV. The distributions, which have been normalized to their charge states for ease of comparison, are indistinguishable. Consequently, we conclude that the angular scatter distribution is independent of the charge state. This results from different interaction mechanisms which govern angular scattering and charge exchange. Angular scattering primarily results from elastic interactions between the transiting projectile and the target atoms. The charge state, however, is determined by inelastic (electronic) interactions which result in electron capture or loss. Since these two mechanisms are independent, the angular scattering and the charge state distributions to likewise be independent.

5. APPLICATIONS TO LENA DETECTION AND CONCLUSIONS

Based on a minimum five percent ionization efficiency LENA detection is viable for hydrogen at energies greater than 1 keV and oxygen greater than approximately 15 keV. Since the LENA hydrogen flux is dominant at all times and the exit charge fraction of H^+ transiting carbon foils is large (5% at 1 keV to 41% at 30 keV) relative to that of oxygen (2% at 10 keV to 8% at 30 keV), LENA instrumentation using a carbon stripping foil should obviously focus on neutral hydrogen detection.

Foils that would be used for LENA sensors would be exposed to air during assembly and testing, and their surfaces will be contaminated. This study shows that air-contamination of Al and Au coated foils is shown to result in identical charge state distributions.

Significant angular scattering of LENAs in the carbon foil will result in loss of information of their incident trajectories or even scattering into instrument walls which prevents their detection. Consequently, knowledge of the scatter distribution is required to define instrument specifications. Deviation in the scattering halfwidth between the empirical results of this study and the theory of Meyer is significant. For hydrogen the scattering halfwidth ranges from approximately 2° at 5 keV to 0.5° at 30 keV, whereas for oxygen the scattering halfwidth is approximately 4°-7°. Due to the large scattering halfwidth for oxygen, high resolution of the incident neutral oxygen trajectory may require use of even thinner (0.2-0.3 $\mu g\ cm^{-2}$) foils, which are currently under study.

Acknowledgements: We gratefully acknowledge J. Baldonado and D. Everett for their laboratory support and D. Deck for Al and Au deposition. This work was performed under the auspices of the United States Department of Energy.

6. REFERENCES

R.W. McEntire and D.G. Mitchell, "Instrumentation for global magnetospheric imaging via energetic neutral atoms", Geophys. Monogr. Ser., Vol. 54, pp. 79-80, 1989.

K.C. Hsieh and C.C. Curtis, "Remote sensing of planetary magnetospheres: Mass and energy analysis of energetic neutral atoms", Geophys. Monogr. Ser., Vol. 54, pp. 159-164, 1989.

D.J. McComas, B.L. Barraclough, R.C. Elphic, H.O. Funsten, and M.F. Thomsen, "Magnetospheric imaging with low-energy neutral atoms", Proc. Natl. Acad. Sci. USA, Vol. 88, pp. 9598-9602, 1991.

A. Burgi, M. Oetliker, P. Bochsler, and J. Geiss, "Charge exchange of low energy ions in thin carbon foils", J. Appl. Phys., Vol. 68, pp. 2547-2554, 1990.

H. O. Funsten, D.J. McComas, and B.L. Barraclough, "Thickness uniformity and pinhole density analysis of thin carbon foils", Nucl. Instr. and Meth. B, in press, 1992.

S. Kreussler and R. Sizmann, "Neutralization of 50-230 keV hydrogen ion which have penetrated Al, Au, C, and Cs films", Phys. Rev B, Vol. 26, pp. 520-529, 1982.

R. Behrisch, W. Eckstein, P. Meischner, B.M.U. Scherzer, and H. Verbeek, "Charged fraction of 5 keV to 150 keV hydrogen atoms after emergence from different metal surfaces", in Atomic Collisions in Solids, Vol. 1 eds. S. Datz, B.R. Appleton, and C.D. Moak (Plenum, New York, 1975) pp. 315-329.

K.H. Berkner, I. Bornstein, R.V. Pyle, and J.W. Stearns, "Charge Fractions and Excited-Atom Populations of 8-100 keV Deuterium Beams Emerging from Solid Films of C, Mg, Nb, and Au", Phys. Rev. A, Vol. 6, pp. 278-288, 1972.

H.D. Betz, "Heavy Ion Charge States", in Applied Atomic Collision Physics, ed. S. Datz (Academic, New York, 1983) pp. 1-42.

L. Meyer, "Plural and Multiple Scattering of Low-Energy Heavy Particles in Solids", Phys. Stat. Sol. (b), Vol. 44, pp. 253-268, 1971.

G. Högberg, H. Nordén, and H.G. Berry, "Angular distributions of ions scattered in thin carbon foils", Nucl. Instr. and Meth., 90, pp. 283-288, 1970.

H.H. Andersen and J. Bøttiger, "Multiple Scattering of Heavy Ions of keV Energies Transmitted through Thin Carbon Foils", Phys. Rev. B, Vol. 4, pp. 2105-2111, 1971.

F. Bernhard, P. Krygel, R. Manns, and S. Schwabe, "Multiple Scattering of Various Ions in Carbon and Germanium", Rad. Eff., Vol. 13, pp. 249-255, 1972.

7. FIGURE CAPTIONS

Fig. 1. Experimental apparatus.

Fig. 2. Equilibrium charge state distributions (O^+ and O^-) as a function of incident ion energy for atomic O^+ incident on a 0.5 $\mu g\ cm^{-2}$ carbon foil.

Fig. 3. Equilibrium charge state distributions (H^+ and H^-) as a function of incident ion energy for atomic H^+ incident on a 0.5 $\mu g\ cm^{-2}$ carbon foil.

Fig. 4. Variation of the H^+ charge state distributions for foils coated with Au and Al relative to an uncoated carbon foil.

Fig. 5. The scatter half-angle ψ as a function of the incident ion energy for hydrogen and oxygen incident on carbon foils of 0.5 $\mu g\ cm^{-2}$ nominal thickness. The solid lines are based on the theory of Meyer and the points are empirical results of this study.

Fig. 6. The scatter distributions of the H^+ and H^0 charge states resulting from the interaction of 20 keV hydrogen with 0.5 $\mu g\ cm^{-2}$ foils. The scatter distributions are virtually indistinguishable, suggesting that scattering and charge exchange result from different projectile-foil interactions.

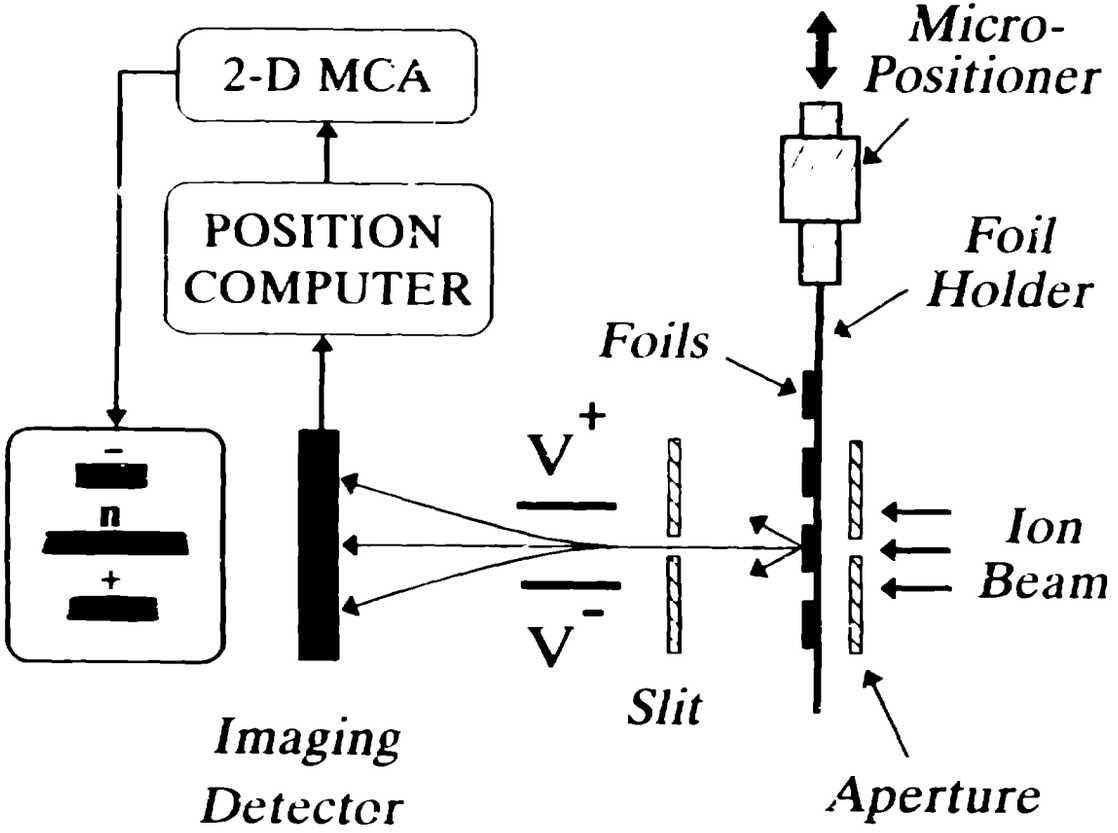
2-D MCA
POSITION COMPUTER
Micro-Positioner
Foil Holder
Foils
V+
V-
Slit
Ion Beam
Imaging Detector
Aperture

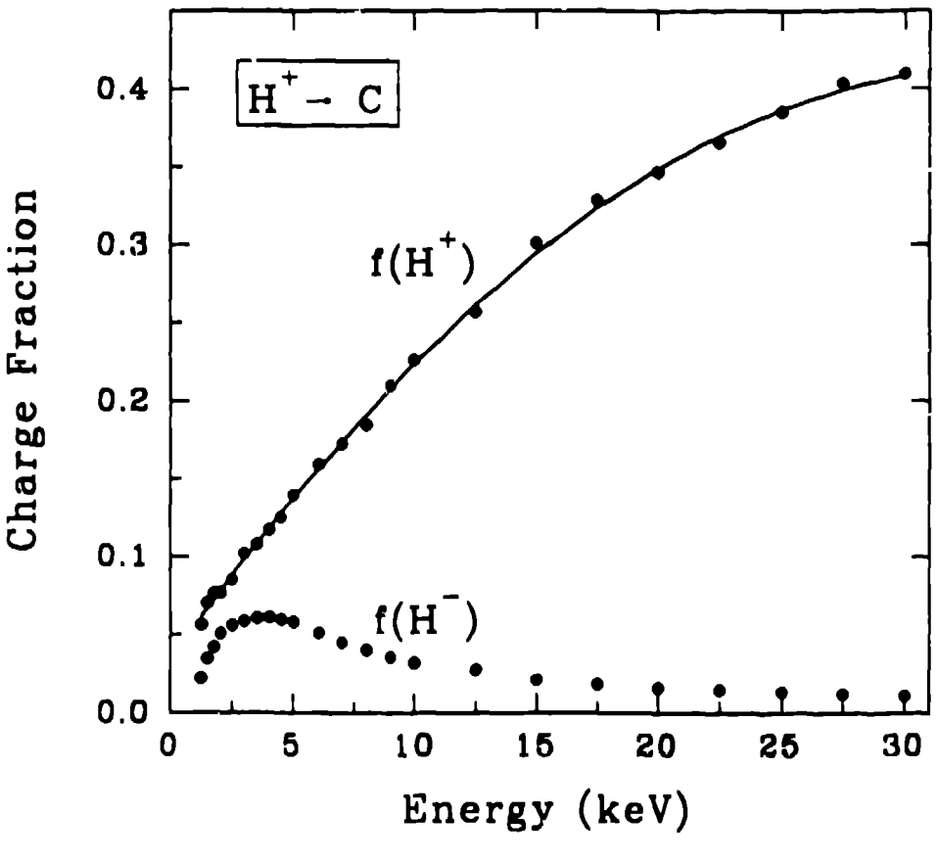
H+ → C
f(H+)
f(H−)
Charge Fraction
Energy (keV)
0.0
0.1
0.2
0.3
0.4
0
5
10
15
20
25
30

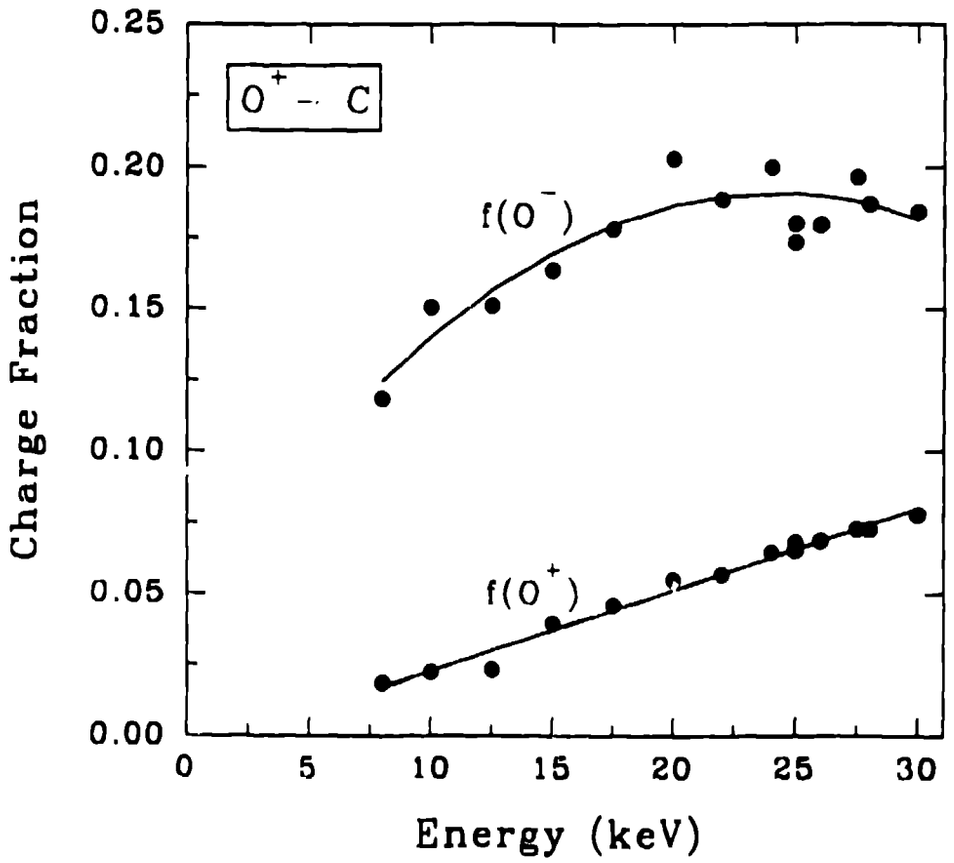
0.25
0.20
0.15
0.10
0.05
0.00
Charge Fraction
O^+ – C
$f(O^-)$
$f(O^+)$
0
5
10
15
20
25
30
Energy (keV)

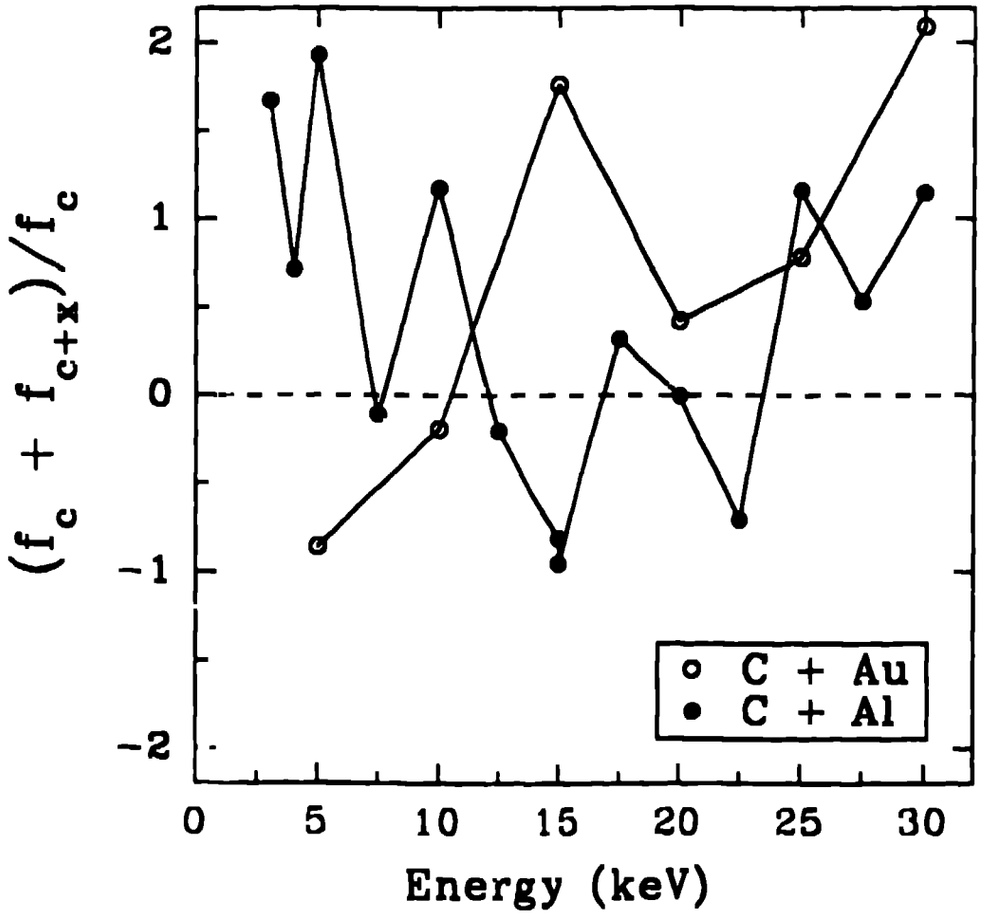
2
1
0
−1
−2
0
5
10
15
20
25
30
Energy (keV)
$(f_c + f_{c+x})/f_c$
C + Au
C + Al

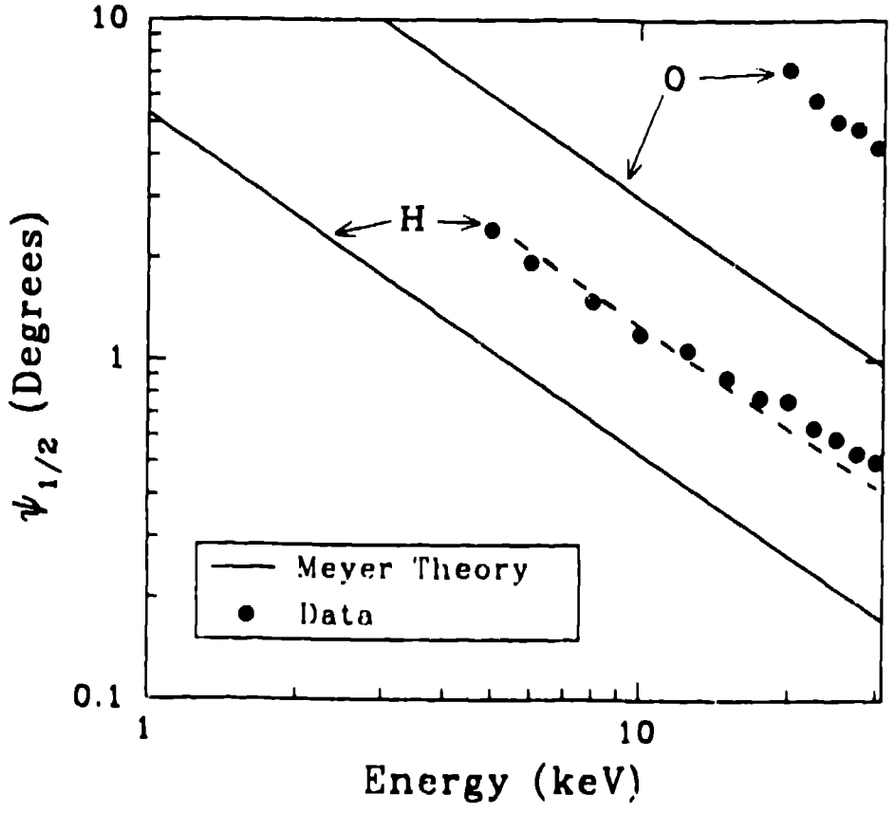
10
1
0.1
1
10
$\psi_{1/2}$ (Degrees)
Energy (keV)
O
H
Meyer Theory
Data

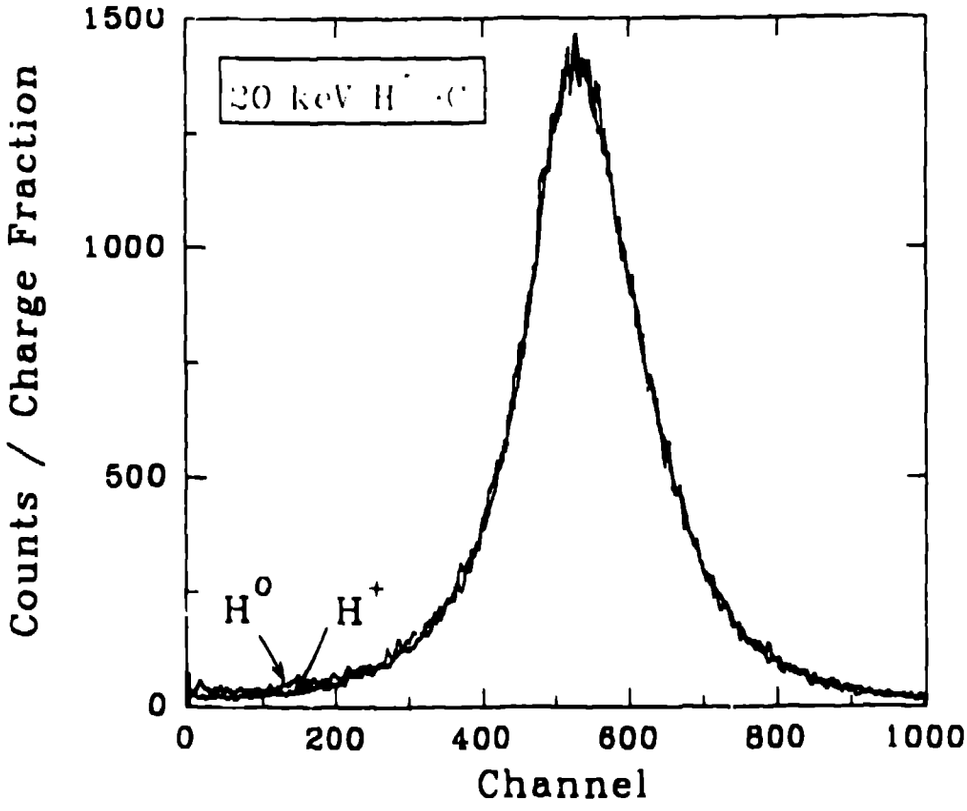

20 keV H⁺ → C
Counts / Charge Fraction
1500
1000
500
0
H⁰
H⁺
0
200
400
600
800
1000
Channel